The dynamic wake of an actuator disc undergoing transient load

A numerical and experimental study
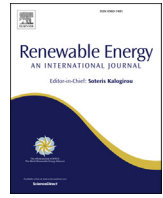
Yu, W.; Ferreira, C.; van Kuik, G. A.M.

Important note
To cite this publication, please use the final published version (if applicable).
Please check the document version above.

The dynamic wake of an actuator disc undergoing transient load: A numerical and experimental study

W. Yu[*], C. Ferreira, G.A.M. van Kuik

Faculty of Aerospace Engineering, Delft University of Technology, Kluyverweg 1, 2629 HS, Delft, the Netherlands

ARTICLE INFO

ABSTRACT

The currently most used theory for rotor aerodynamics — Blade Element Momentum is based on the assumption of stationary wake conditions. However, an unsteady rotor loading results in an unsteady wake flow field. This work aims to study the impact of an unsteady actuator disc on the wake flow field using a free wake vortex ring model. The numerical results are compared to a wind tunnel measurement, where the wake flow of an actuator disc model undergoing transient load was obtained. The numerical results complement the experimental work while providing information such as the vorticity field and contributions from different vortex elements. The velocity at different locations is compared between the experimental and numerical results. The observed velocity peaks in the experimental results are also observed in the numerical results. A steeper ramp time results in a steeper velocity transient slope, and in turn in a larger amplitude of peak values. It is revealed that the rolling-up processes is the main cause for the velocity difference at various locations and in the three cases by decomposing velocity induced by different vortex element.

1. Introduction

Currently, the widely utilized theory for rotor aerodynamics — Blade Element Momentum (BEM) is based on the assumption of stationary wake conditions. However, an unsteady rotor/actuator loading results in an unsteady wake flow and induction field, commonly named 'Dynamic inflow' or 'Dynamic wake'.

The concept of actuator disc (or momentum or slip-stream) is the first mathematical representation of a screw propeller, aircraft propeller or wind turbine rotor [1], which was introduced by Froude [2]. This concept is the basis of BEM. A huge amount of research focuses on steady and unsteady actuator disc by analytical, numerical and experimental approaches. Analytical formulae of the velocity field induced by a steady straight cylindrical wake of a uniformly loaded actuator disc were obtained by Callaghan and Maslen [3], Gibson [4], van Kuik and Lignarolo [5], and Branlard and Gaunaa [6] using different approaches. Conway [7] obtained a linear solution for an actuator disc with steady radial varied heavy loads by using a self-conserving vortex system. The velocity singularity at the edge of an actuator disc with constant normal load

was mathematically addressed by van Kuik [8].

The character of the velocity singularity at the edge of an actuator disc can be represented by a discrete vortex ring system in numerical ways. A wake model consisting of a system of vortex rings was developed to calculate the thrust and the induced velocity of a uniformly loaded rotor disc by Øye [9]. The induction of an actuator disc with steady thrust from BEM was compared with CFD analysis by Madsen [10]. The axi-symmetric actuator disc model combined with the incompressible Navier-Stokes equations was applied to investigate the aerodynamics of wind turbine rotors by Mikkelsen [11]. The near wake of a steady actuator disc was shown to be predicted better by a vortex model over four large eddy simulation (LES) codes by Lignarolo et al. [12], when compared with experimental results.

The unsteady wake development of an actuator disc (or a flat plate) undergoing impulsive motion in the flow direction was studied numerically by Koumoutsakos and Shiels [13], Higuchi and Balligand [14]. Higuchi and Balligand [14] observed a vortex ring structure in the wake of a disc during an acceleration and a counter-rotating vortex ring structure during a deceleration using a vortex model. Koumoutsakos and Shiels [13] quantitatively analysed the vorticity and force generated by a flat plate undergoing an impulsively started motion normal to the free stream direction, using a two-dimensional viscous incompressible model. Both studies

showed that the vortex ring structures form at the edge of the disc or plate shortly after the load change. The size of the ring-like vortical structures increase with time but the spatial position adheres to the body edge. Secondary vortices were also observed at the back of the disc by Koumoutsakos and Shiels [13] and Higuchi and Balligand [14].

The wake development of an actuator disc undergoing transient loads was investigated experimentally using a disc model with variable porosity in Yu et al. [15]. A free wake vortex ring (FWVR) model which can account for the induced velocity field of any radial varied and unsteady loaded actuator disc was developed by Yu et al. [16]. This paper aims to compare the wake field of an actuator disc undergoing transient load with the wind tunnel measurements from Yu et al. [15] and numerical results calculated from the FWVR model [16]. The induction from different vortex elements, vortex shed before and after the load change and the rolled-up vortex, is decomposed to explain the physics behind the velocity overshoot/undershoot, to discover the difference between the three reduced ramp time cases, and the difference between load increase and decrease cases.

The understanding of dynamic wake development of an actuator disc undergoing transient load in this work has practical importance. For example, the knowledge of the phase delay and time constants of the transient process can help improve the design of pitch control algorithms.

This paper is structured as follows. Section 2 introduces the methods used in this paper, including a brief description of the FWVR model and the experimental test cases. Sections 3 and 4 present the results and discussions for steady and unsteady load cases, respectively. The wake velocity profiles are compared between the numerical and the experimental results. The key observations in velocity are explained by decomposing the velocity induced by different vorticity elements of the FWVR model for the unsteady cases. Section 5 presents the main conclusions.

2. Methods

2.1. Free wake vortex ring model

The free wake vortex ring model developed in Yu et al. [16] is used for this study. In this model, the near wake is modelled by dynamic surfaces, consisting of free vortex rings shed from the edge of the actuator disc. The far wake is represented by a semi-infinite cylindrical vortex tube with constant strength and radius. The vortex rings are considered thin, axisymmetric and uniform. In this axisymmetric loaded actuator disc study, vortex rings expand or contract, while their central axis always coincides with the axis of the actuator disc. The scheme of a cut-off is used to remove the singularity. No viscous diffusion is considered in the model. Since the wake after around 5D is frozen and represented by a vortex tube, the model cannot model wake meandering. The Lagrangian formulation of this model is particle based without an underlying grid. No turbulence model is applied.

The relationship between the strength of the new vortex ring generated during time Δt and the corresponding C_t is given by

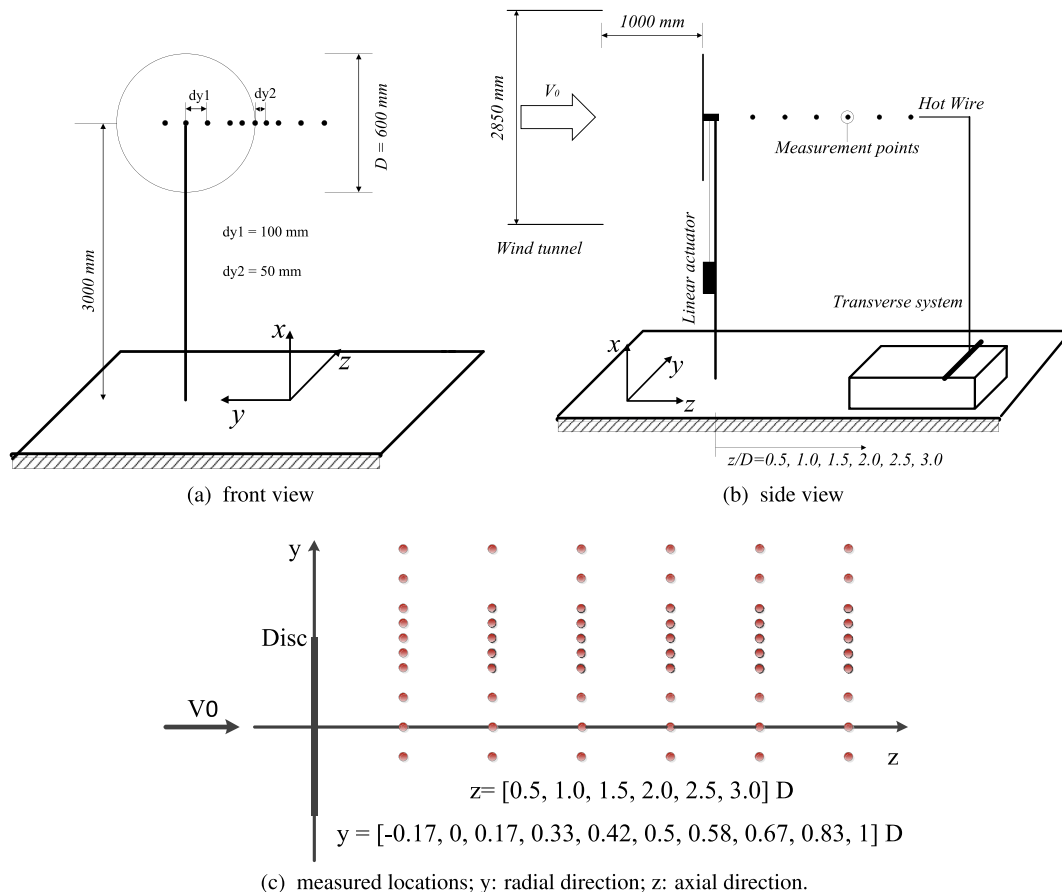$$\Gamma = C_t \left(\frac{1}{2} V^2 \right) \Delta t. \tag{1}$$

Fig. 1. Schematic of the experimental set-up and locations of velocity measured downstream the disc (Yu et al. [15]).
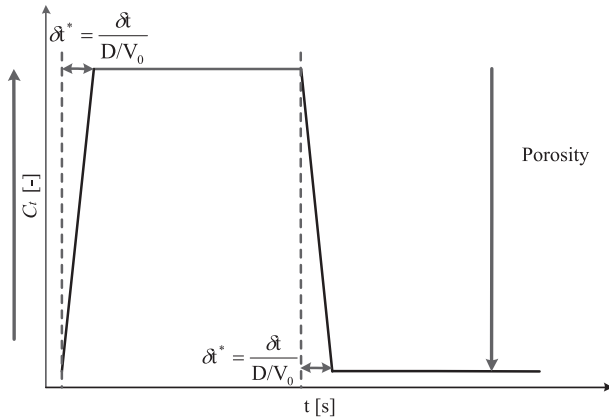
Fig. 2. Unsteady load profile (Yu et al. [15]).

Table 1
Tested steady and unsteady cases.

Cases	number	porosity [%]	thrust	δt^*
Steady cases	SI	69.4	$C_t^{low} = 0.767$	–
	SII	44.4	$C_t^{high} = 0.933$	–
Unsteady cases	UI	44.4 → 69.4	$C_t^{high} \rightarrow C_t^{low}$	0.2
	UII	44.4 → 69.4	$C_t^{high} \rightarrow C_t^{low}$	0.4
	UII	44.4 → 69.4	$C_t^{high} \rightarrow C_t^{low}$	0.8

A time step of $\Delta\tau = 0.05$ and a cut-off radius of $\delta = 1 \times 10^{-5}$ are chosen for the simulations. The effect of time step and the cut-off radius are presented in Yu et al. [16]. The prediction of steady velocity field from the FWVR model is validated against an actuator disc experiment, which is also given in Yu et al. [16].

2.2. Experimental cases

The information on the experimental cases is shortly repeated here. More details can be found in Yu et al. [15].

A schematic representation of the front and side view of the experimental set-up is shown in Fig. 1(a) and (b), respectively. The load on the disc is varied through adjustment of the relative open area (porosity) formed by two identical parallel porous discs. Each disc has a diameter of 600 mm. The velocity field at planes of 0.5D to 3.0D with an interval of 0.5D is measured by a hot-wire anemometer. Fig. 1(c) depicts the measurement locations taken during the experiments.

To represent pitching transients of a wind turbine, a ramp change profile is prescribed in all unsteady cases (see Fig. 2), with δt representing the ramp time. The reduced ramp time (δt^*) is used in this experiment, which is defined by equation (2).

$$\delta t^* = \frac{\delta t}{D/V_0} \tag{2}$$

In addition to the two steady cases corresponding to the two steady porosity states, three different reduced ramp times, $\delta t^* = 0.2, 0.4, 0.8$, are tested for the unsteady cases in the experiment. The steady and unsteady tested cases are summarized in Table 1.

Fig. 3 gives the filtered thrust coefficient for the three cases measured by the load cell. The measured ramp time of both the filtered and unfiltered load signals are not only due to the aerodynamic effect because the existence of the dynamic response of the entire mechanical system. More details about the effect of the
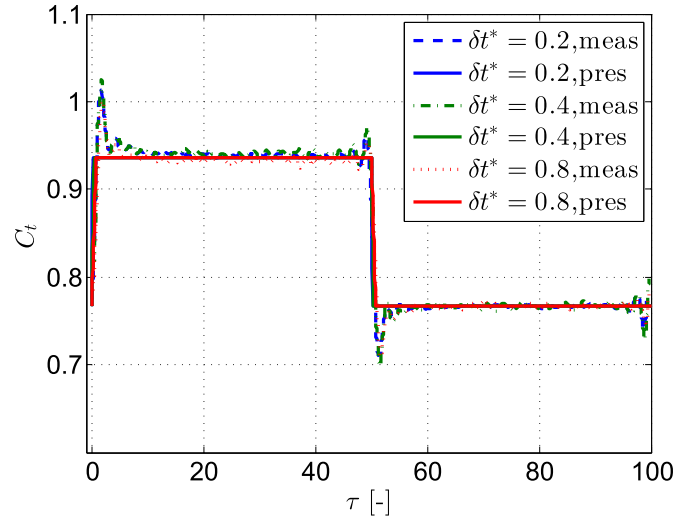

Fig. 3. The filtered experimental measured thrust (meas) and the prescribed thrust (pres) for the three unsteady cases. The prescribed thrust serves as input for the simulations.

systematic vibration is discussed in reference Yu et al. [15]. Therefore, the load change profiles are assumed to change at the same reduced ramp time as the porosity change, which are plotted as solid lines in Fig. 3. These prescribed thrust profiles, instead of the directly measured ones, serve as input for the numerical simulation of the FWVR model.

3. Results and discussion of steady cases

Fig. 4 compares the measured axial velocity profiles with those from the FWVR model at the six downstream planes for the two steady cases. Overall, the steady velocity profiles predicted by the FWVR model track the experimental measurements. At $y/D = 0$, the velocity deficit from the experimental results is larger due to the additional blockage effect from the nacelle in the experiments. This effect from the nacelle decreases as the plane moves downstream. The discrepancy between the numerical and experimental results is larger for the wake boundary shear layer region, which might be caused by two factors. The first factor is that no viscous diffusion is modelled in the FWVR model. The other one is that the shear layer region where the vortex elements concentrate is prone to the dynamic effects of vortex roll-up, as shown in Figs. 5 and 6. The increase of the shear layer region as it goes further downstream owes to the development of the wake expansion.

4. Results and discussion of unsteady cases

A number of locations in the wake as shown in Fig. 1(c) have been measured. Velocity at seven locations is presented, which highlight the characteristics of the flow downstream the disc. They are located inside the inner wake ($y/D = 0.33$), outside the wake ($y/D = 0.83$) and in the shear layer ($y/D = 0.58$) of three planes $z/D = 1.0, 2.0$ and 3.0, which are summarized in Table 2.

The comparison of the velocity in the wake under the steady load has been shown in section 3. The analysis of flow under unsteady conditions focuses on the transient wake changes instead of comparing the steady state values. Therefore, the axial velocity is presented in a non-dimensional way using
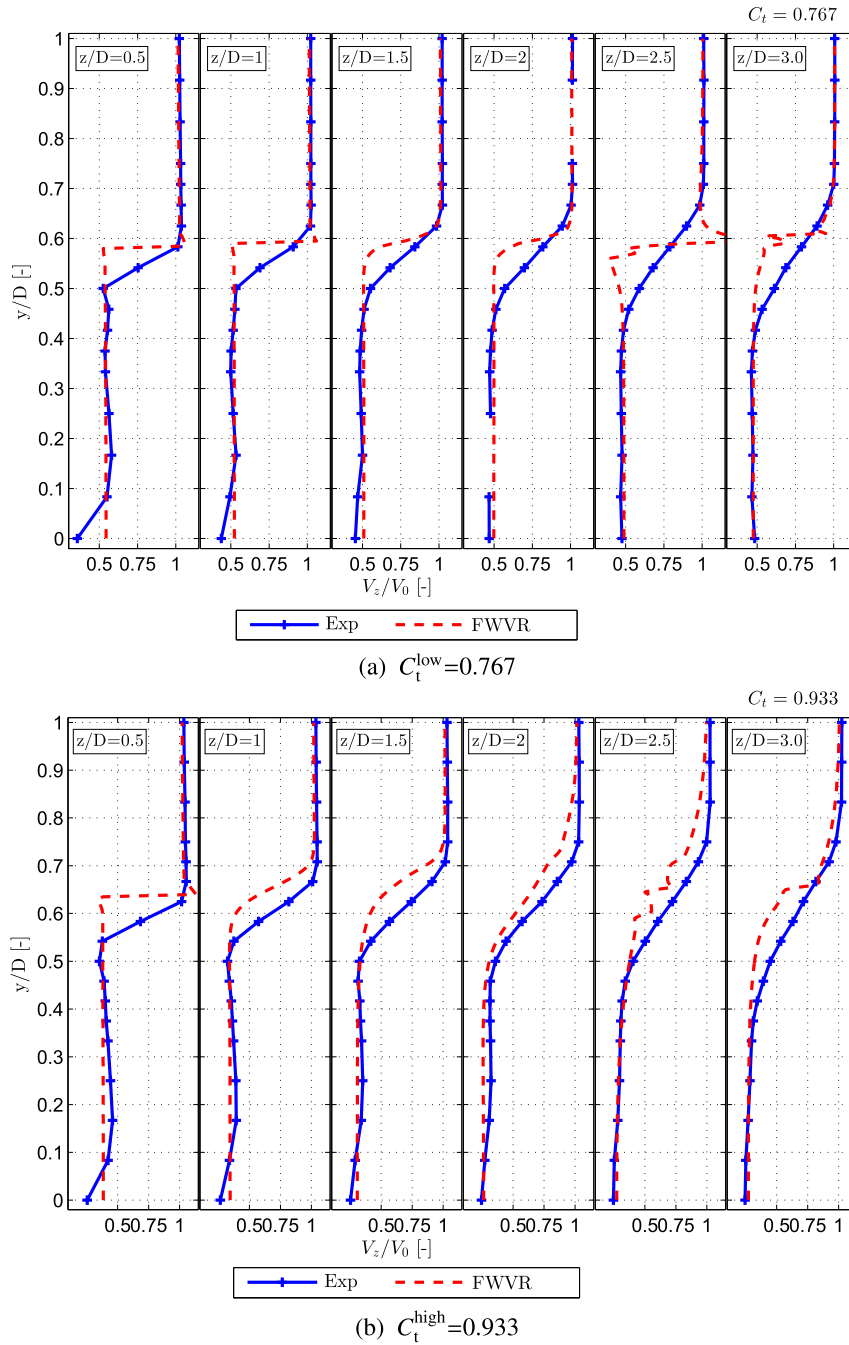
(a) C_t^{low}=0.767

(b) C_t^{high}=0.933

Fig. 4. Comparison of normalized axial velocity at different downstream locations under steady load between experiments and the FWVR model.

$$\widetilde{\Delta V_z} = \frac{V_z - V_{z,s1}}{V_{z,s2} - V_{z,s1}}. \tag{3}$$

where V_z is the instantaneous axial velocity. The subscripts $s1$ and $s2$ represent the initial (before load change) and the final steady state (sufficient time after load change) values.

For the transient velocity profile comparison in subsection 4.1 and 4.3, the self-normalized transient responses from the experimental and numerical results are used. For the comparison of effect from different vortex elements in subsection 4.2 and 4.4, the absolute induced velocity from each vortex element is used. The time presented in the results is non-dimensionalized to the dynamic

inflow time scale using $\tau = \frac{V_0 t}{D}$.

4.1. Dynamic wake for the load case $\delta t^* = 0.2$

Take the load case $\delta t^* = 0.2$ as an example, this section compares the velocity at different locations between the numerical and experimental results.

Fig. 5 shows the development of the wake after load increase. Locations of the intersections of the vortex rings with the symmetry plane from the FWVR model are plotted at time $\tau = 0.5$, 1.0, 1.5, 2.0, 3.0, 6.0. The vortices shed before and after the onset of load change from the FWVR model are presented by particles with light and dark color, respectively. Fig. 6 shows the wake development
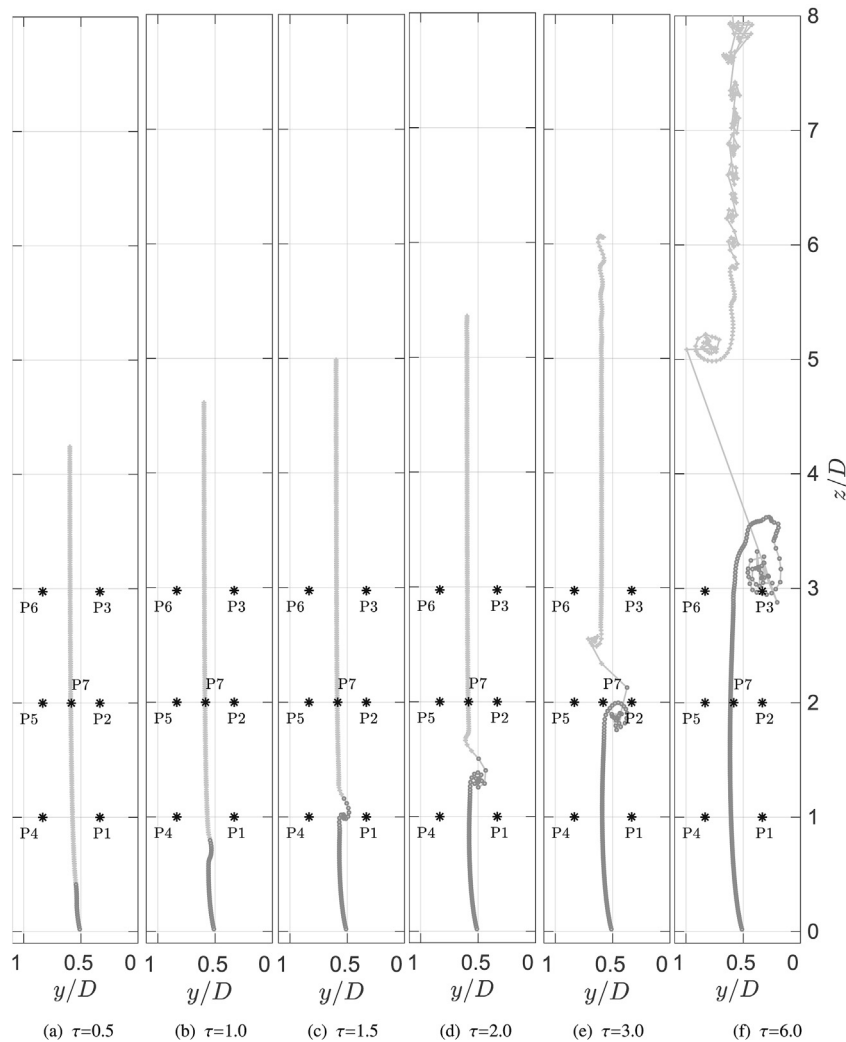
Fig. 5. Wake development after load increase calculated by the FWVR model (dark and light particles represent vortices shed after and before load change, respectively).

after load decrease.

It can be seen in Fig. 5, under the interaction of the vorticity shed before and after the load increase, the vortex sheet starts to move inward and roll up. An inward knot is noticeably formed when comparing the plot at $\tau = 1.5$ to that at $\tau = 1.0$. As the vorticity accumulates, the knot gradually rolls into a ring-like vortical structure. This is different from the fully loaded disc cases observed in literature [13,14,17,18], where the vorticity rolls up at the edge of the disc shortly after the impulsive motion and maintains attached to the disc while growing up into ring-like vortical structures. Remarkably, as shown in Fig. 6, the vortex sheet starts to move outward and roll up under the interaction of the vorticity shed before and after load decrease. An outward knot is observably formed when comparing the plot at $\tau = 1.5$ to that at $\tau = 1.0$. Eventually, the knot rolls into a big ring-like vortical structure. The roll-up vortical structure moves outwards and is also convected downstream at the same time.

Fig. 7 shows the velocity development from the experiment and the FWVR model at P2, P7 and P5, after load increase and decrease. The velocity at the three radial positions from the same downstream plane starts to respond simultaneously to the load variation at around $\tau = 2$, for both load increase and decrease cases. From the experimental results, the turbulence is higher in the shear layer region at P7 in both the load increase and decrease cases. Due to the

velocity singularity induced by the vorticity when the observed locations are too close to the vortex elements, the result from the FWVR model is highly influenced by the vorticity elements in the shear layer region.

For the load increase case, it can be seen that with the entire vortex system convecting downstream, the velocity decreases eventually to the new steady state of the higher disc load at the inner wake $y/D = 0.33$ and the shear layer $y/D = 0.58$. The eventual decrease of velocity inside the wake corresponds to the higher induction at this higher disc load state. The velocity at the outer wake $y/D = 0.83$ eventually increases to the new steady state. The final increase of velocity attributes to the larger blockage effect of the disc at the higher disc load; and vice versa for the load decrease case.

The undershoot/overshoot of the velocity before the new steady state is also observed from the numerical results. This is presumed to be caused by the rolling-up process of the vortex and its relative positions to the observed positions during its passage, which will be verified in subsection 4.2.

Comparing Figure 7(a) to Figure 7(b), there is a larger overshoot/undershoot at P2 for the load increase case than that for the load decrease case. Conversely, there is a larger overshoot/undershoot at P5 for the load decrease case than that for the load increase case, for both experimental and numerical methods. This will be further
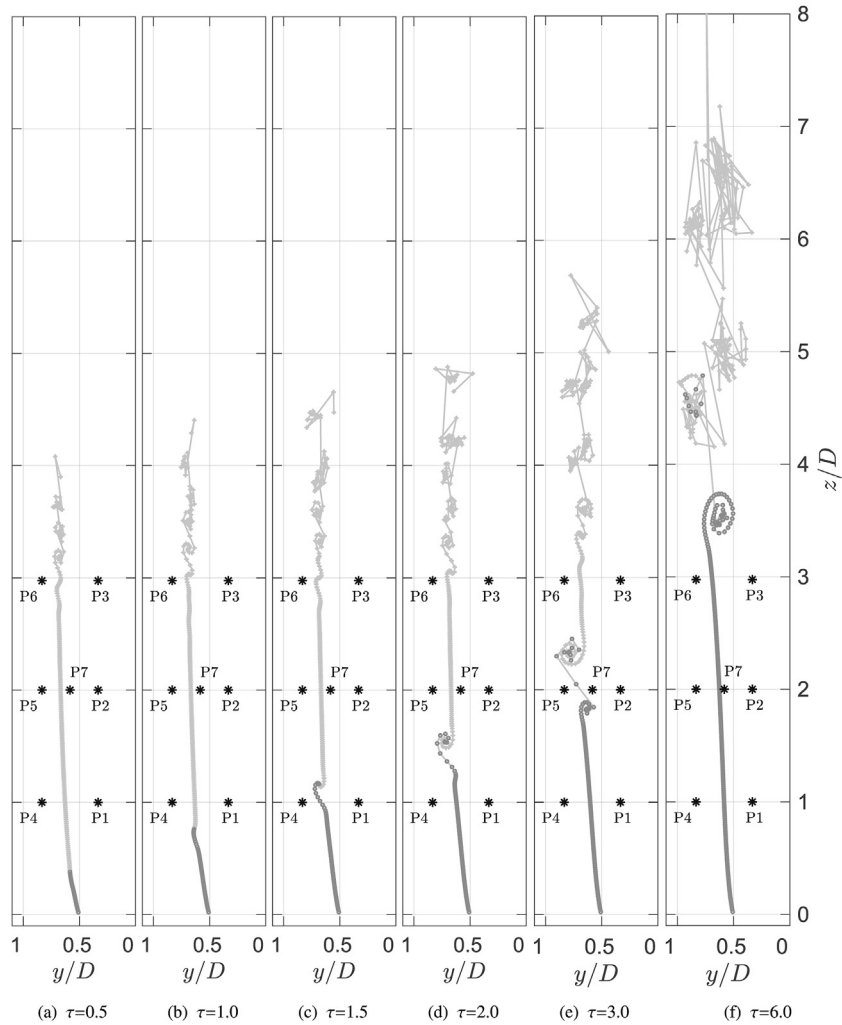
Fig. 6. Wake development after load decrease calculated by the FWVR model (dark and light particles represent vortices shed after and before load change, respectively).

Table 2
Locations in the wake of the discussed positions.

Position	P1	P2	P3	P4	P5	P6	P7
z/D	1.0	2.0	3.0	1.0	2.0	3.0	2.0
y/D	0.33	0.33	0.33	0.83	0.83	0.83	0.58

explained in subsection 4.2.

The velocity development from both methods at the locations P1, P2 and P3 after load increase and decrease are presented in Fig. 8. From Fig. 8(a) and (b), the time onset of velocity response at the same radial positions but different planes upon the onset of load change are different - the velocity starts to perturb at $\tau = 1.0$ for P1, at around $\tau = 2.0$ for P2, at around $\tau = 3.0$ for P3. As the flow disturbance convects downstream, the velocity field at locations from the near wake to the far wake starts to respond successively. The comparison of the velocity profiles at these locations between the load increase and decrease cases shows that there is a larger secondary unsteadiness effect in the load increase case than that in the load decrease case. This holds for both experimental and numerical results.

Fig. 9 presents the velocity development at the P4, P5 and P6 after load increase and decrease. As similar as locations at $y/D = 0.33$ on these planes in Fig. 8, the velocity starts to perturb at

around $\tau = 1.0$ for P4, at around $\tau = 2.0$ for P5, at around $\tau = 3.0$ for P6. It shows that the velocity overshoot/undershoot increases as the plane goes further downstream for both load increase and decrease cases for both methods. On the contrary to the velocity at $y/D = 0.33$ in Fig. 8, the secondary unsteadiness effect is larger in the load decrease case than that in the load increase case at the locations of $y/D = 0.83$; this holds for both methods. The relatively larger velocity overshoot/undershoot at P5 and P6 from the numerical results in Fig. 9(b) is caused by the outwards moving roll-up vortical structure in this load case. As indicated in Fig. 11(b), the observed location P5 and P6 is already at the core of the roll-up structure, which results in the relative large velocity transient.

Figs. 8 and 9 show that the turbulence of the measured velocity is greater in the load increase case than that in the load decrease case. This is caused by the distance of the measurement position to the wake boundary shear layer. This distance depends on the wake expansion. The radial positions of $y/D = 0.33$ and $y/D = 0.83$ are closer to the shear layer at the high thrust when the wake expansion is larger, which is also can be seen in Fig. 4. The turbulence is greater in the further downstream planes also indicates the growth of wake expansion. As explained in subsection 2.1, the FWVR can not capture the turbulence. Additionally, the fixed frequency of the velocity in Figs. 7–9 is caused by the vortex shedding experienced by the disc wire mesh at the edge, which can be described by the
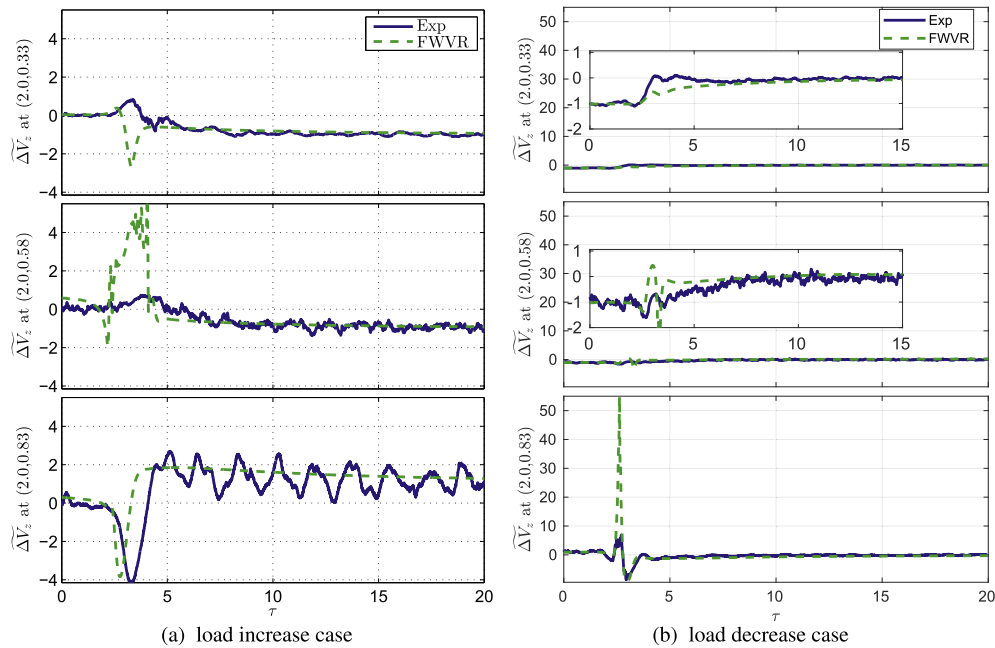
Fig. 7. Velocity at P2 (z/D=2.0, y/D = 0.33), P7 (z/D=2.0, y/D = 0.58), P5 (z/D=2.0, y/D = 0.83) from experiment and the FWVR model in load increase and decrease cases.
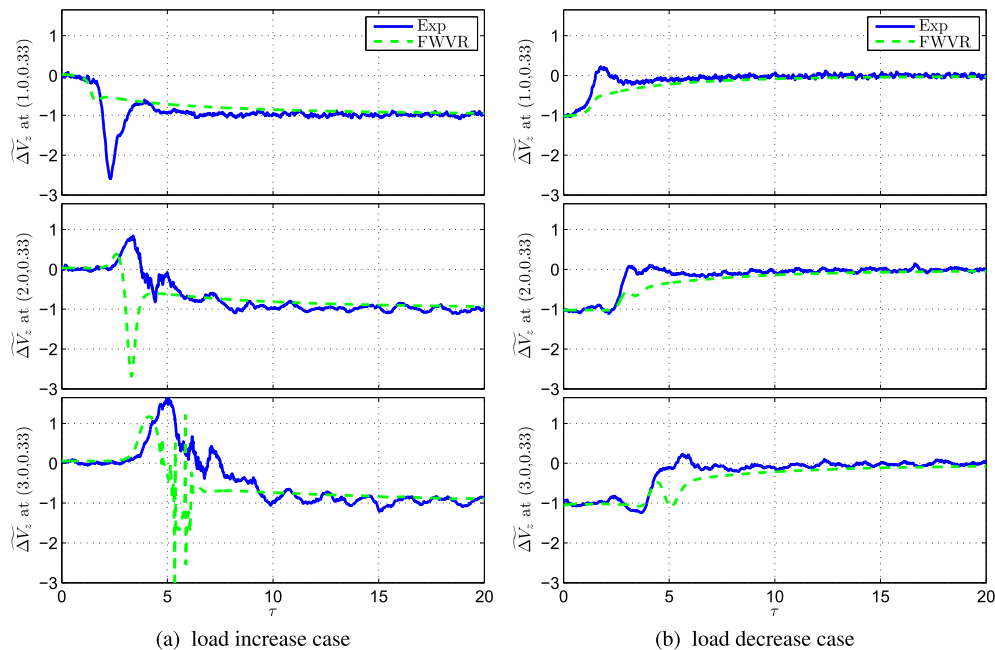

Fig. 8. Velocity at P1 (z/D=1.0, y/D = 0.33), P2 (z/D=2.0, y/D = 0.33), P3 (z/D=3.0, y/D = 0.33) from experiment and the FWVR model in load increase and decrease cases.

Strouhal number.

It can be seen in Figs. 7–9 that although there are some local magnitude differences for the overshoots/undershoots, the numerical model can reasonably capture the experimental dynamic velocity profiles at different locations in the field, in terms of the secondary velocity unsteadiness and the transient profile. The transient response includes the time to start to respond to the disturbance and the time it takes to reach the new steady state.

The difference in overshoot/undershoot between the numerical and experimental results, e.g., the opposite overshoot at P2 in the load increase case in Fig. 8(a), is likely caused by the lack of mesh

details of the vortex simulation. Specifically, the effect of tower and holes of disc mesh is present in the experiment, which is not taken into account in the simulations. The effect of the systematic mechanical vibration is another reason, whose effect is unknown. It cannot be totally isolated from the aerodynamic effect in the experiment.

4.2. Decomposed velocity analysis of case $\delta t^* = 0.2$

Section 4.1 shows the secondary unsteadiness — velocity overshoot/undershoot in the wake caused by the dynamic load change
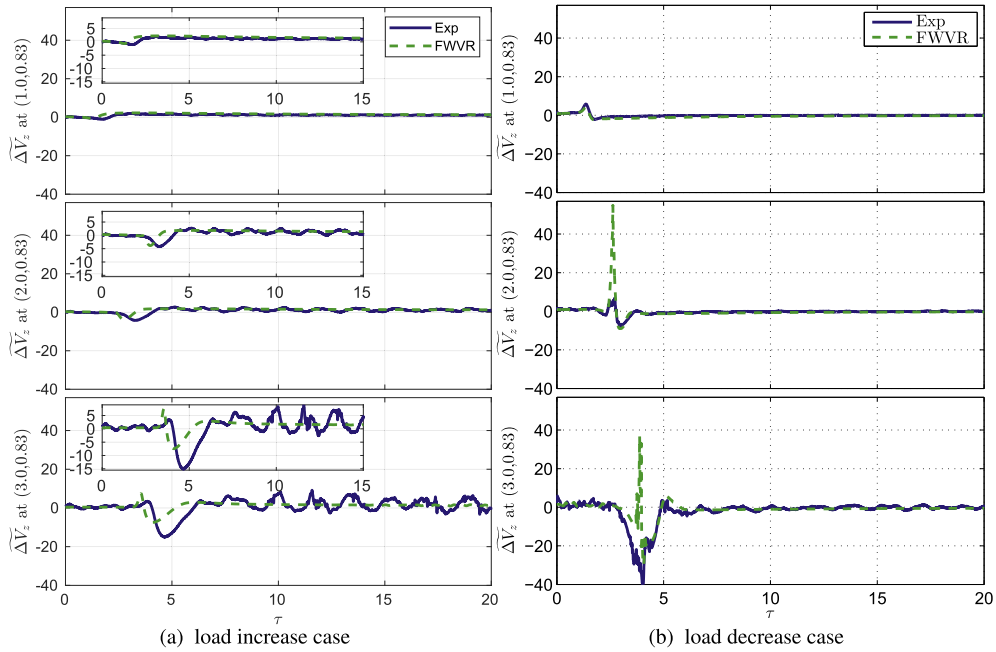
Fig. 9. Velocity at P4 (z/D=1.0, y/D = 0.83), P5 (z/D=2.0, y/D = 0.83), P6 (z/D=3.0, y/D = 0.83) from experiment and the FWVR model in load increase and decrease cases.
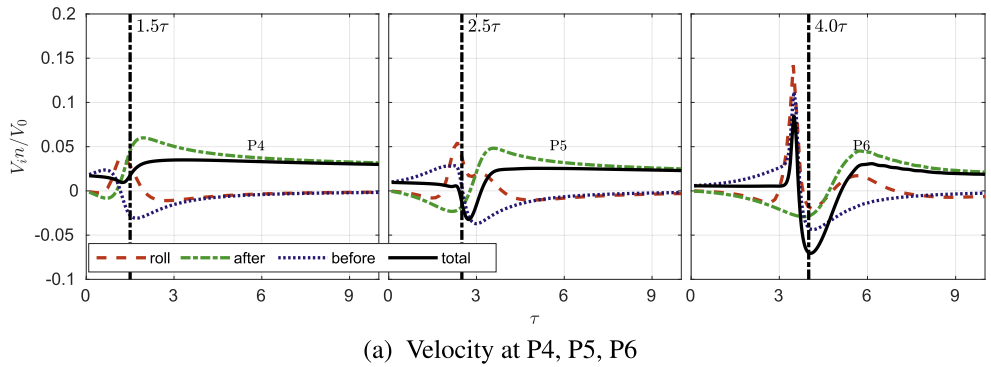
(a) Velocity at P4, P5, P6
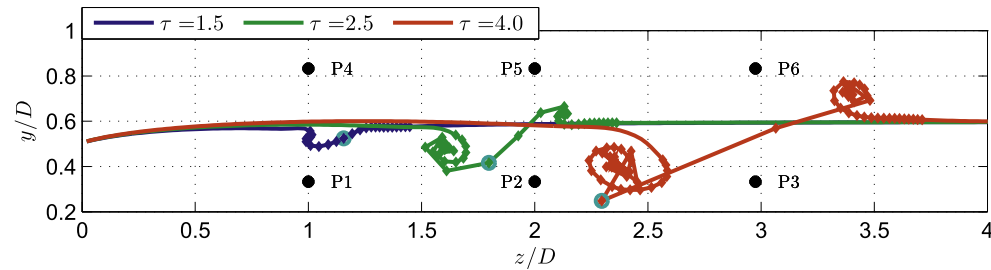
(b) vortex position at time τ=1.5, 2.5, 4.0
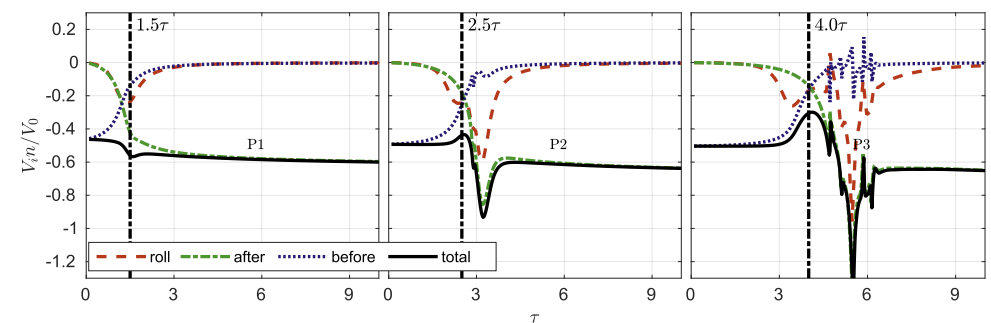
(c) Velocity at P1, P2, P3

Fig. 10. The velocity induced by the vorticity shed before and after load change, the rolled-up vorticity and the total at P1−P6 and wake of the FWVR model at time step τ = 1.5, 2.5, 4.0 for load increase of case $\delta t^* = 0.2$.

(a) Velocity at P4(z/D=1, y/D=0.83), P5(z/D=2, y/D=0.83), P6(z/D=3, y/D=0.83)

(b) vortex position at time τ=1.5, 2.5, 4.0

(c) Velocity at P1(z/D=1, y/D=0.33), P2(z/D=2, y/D=0.33), P3(z/D=3, y/D=0.33)

Fig. 11. The velocity induced by the vorticity shed before and after load change, the rolled-up vorticity and the total at P1–P6 and wake of the FWVR model at time step $\tau = 1.5$, 2.5, 4.0 for load decrease of case $\delta t^* = 0.2$.

on the disc, where it is assumed that the abrupt velocity change is caused by the rolling-up process of the vorticity and its subsequent passage downstream.

In this section, the assumption will be verified by decomposing the velocity induced by different vorticity elements from the FWVR model, using case $\delta t^* = 0.2$ as an example. Fig. 10(b) plots the positions of the vortex rings at time $\tau = 1.5$, 2.5 and 4.0 after load increase. The vorticity shed before and after the onset of load change are divided by the circular mark. The rolled-up vorticity is counted from the first vortex element shed when the load starts to change, with one increment at each side of vorticity shed before and after the load change in every $0.125\tau_0$, as marked with diamonds in Fig. 10(b). The three time corresponding to the vorticity plotted in Fig. 10(b) are also marked by the vertical dash line accordingly in Fig. 10(a) and (c). It can be seen these are the time around when the velocity peaks at these planes. Fig. 10(a) and (c) shows the velocity induced by the vorticity shed before and after the load change, and the rolled-up vorticity and the total at locations P4–P6 and P1–P3, respectively, for load increase case. These locations are also marked in Fig. 10(b).

As the rolled-up vorticity is convected downstream, the induced velocity from the rolled-up vorticity at the three planes peaks around $\tau = 1.5$, 2.5, 4.0 accordingly for both $y/D = 0.83$ and 0.33. As the rolled-up vorticity grows when it is being convected, the amplitude of the peak velocity induced by the rolled-up vorticity increases with downstream planes. The increased peak of the velocity induced by the roll-up vorticity results in an increase peak in the total velocity from $x/D = 1$ to $x/D = 3$. This explains the increase amplitude of overshoot/undershoot when the planes moves downstream in Figs. 8 and 9. The further downstream the plane is, the larger extent of accumulation of vortices is, which results in a larger amplitude of velocity overshoot/undershoot.

It is shown in Fig. 10(a) and (c) that the rolled-up vorticity has a larger effect on the inner wake $y/D = 0.33$ than the outer wake $y/D = 0.83$. This is because of the inward movement of the rolled-up vorticity in the load increase case. The total velocity peaks at the time when the velocity induced by the rolled-up vorticity peaks in Fig. 10(c). However, this is not the case for P4 and P5 in Fig. 10(a). This explains the larger overshoot/undershoot at P1, P2 and P3 in the load increase case than that in the load decrease case in Fig. 8.
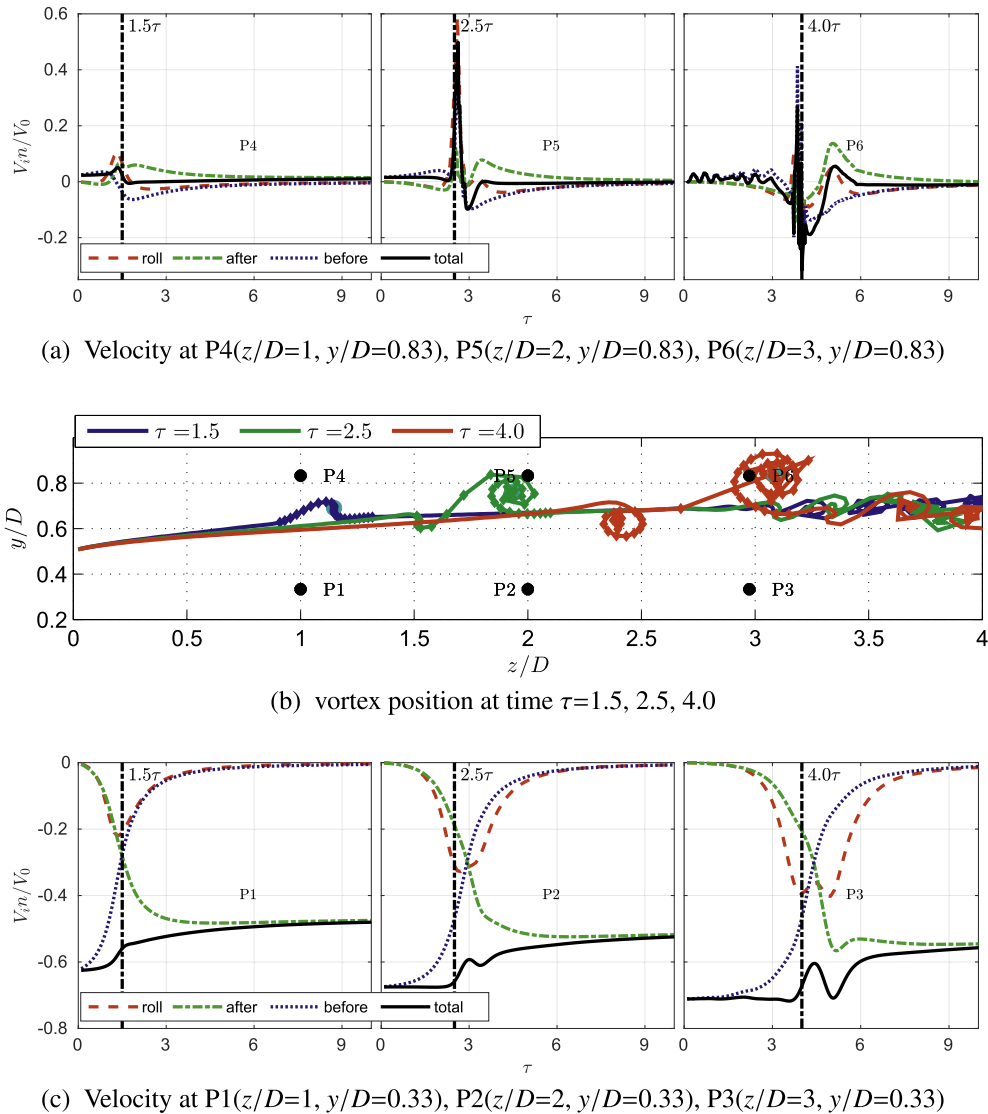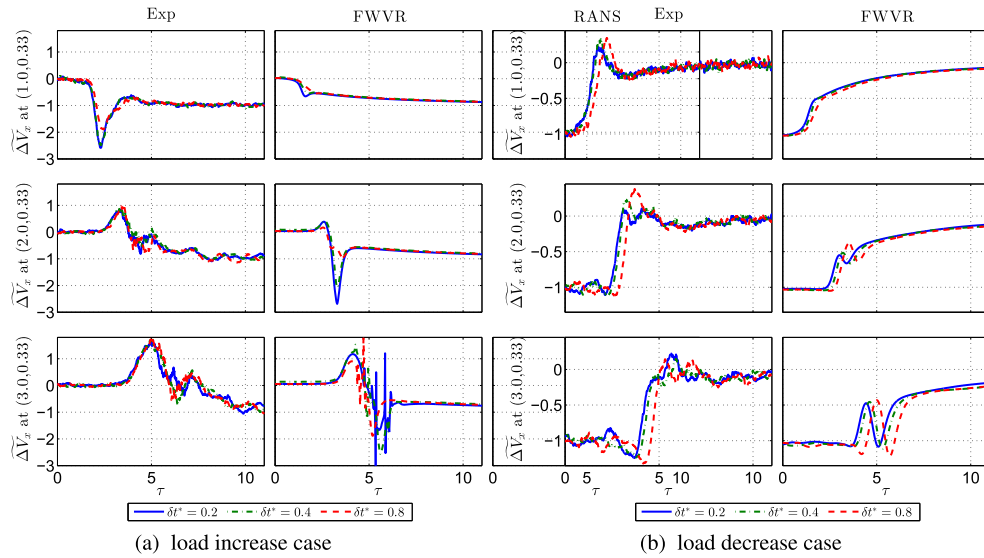
Fig. 12. Velocity at P1 ($z/D=1$, $y/D=0.33$), P2 ($z/D=2$, $y/D=0.33$), P3 ($z/D=3$, $y/D=0.33$) from experiment and the FWVR model in load increase and decrease cases for $\delta t^* = 0.2$, 0.4, 0.8.

The velocity induced by the vortex shed after load change at P4 − P6 firstly decreases before increasing to a peak, and then slowly decays to a converged value. Despite the vortex shed after load change accumulated with time, it starts to roll up before reaching these positions. The roll-up process moves the vorticity away from these positions, resulting in a temporal decrease in induced velocity. Combining it with the contribution from the vortex shed before load change, it leads to an undershoot in the total velocity at these locations. The overshoot at P6 is caused by its short distance to part of the rolled-up vorticity, as shown in Fig. 10(b).

Fig. 11(b) plots the vorticity position of the vortex rings at times $\tau = 1.5$, 2.5 and 4.0 after load decrease. Fig. 11(a) and (c) show the velocity induced by the vortex shed after and before load change, and the rolled-up vorticity and the total at locations P4−P6 and P1−P3 respectively, for load decrease case. The induced velocity from the rolled-up vorticity at the three planes also peaks around

$\tau = 1.5$, 2.5, 4.0 accordingly for both $y/D = 0.83$ and 0.33 in this load decrease case. The peak amplitude of the velocity induced by the rolled-up vorticity increases with downstream planes with an exception of P6. P6 is sensitive to the vortex elements as it is inside the rolled-up vorticity, as seen in Fig. 11(b). At $\tau = 1.5$, the peak amplitude of the induced velocity by the rolled-up vorticity at P4 is still low because the rolling-up process just starts. Consequently, the total velocity curve has a slight peak. This explains the increase amplitude of overshoot/undershoot when the planes moves downstream in Fig. 9.

As plotted in Fig. 11(b), in this load decrease case, the accumulated rolled-up vorticity moves outwards, closer to the locations in the outer wake $y/D = 0.83$. The total velocity peaks at where the velocity induced by the rolled-up vorticity peaks for P4–P6. This is not the case for the locations at $y/D = 0.33$ P1−P3 in Fig. 11(c), as the accumulated rolled-up vorticity moves away from these
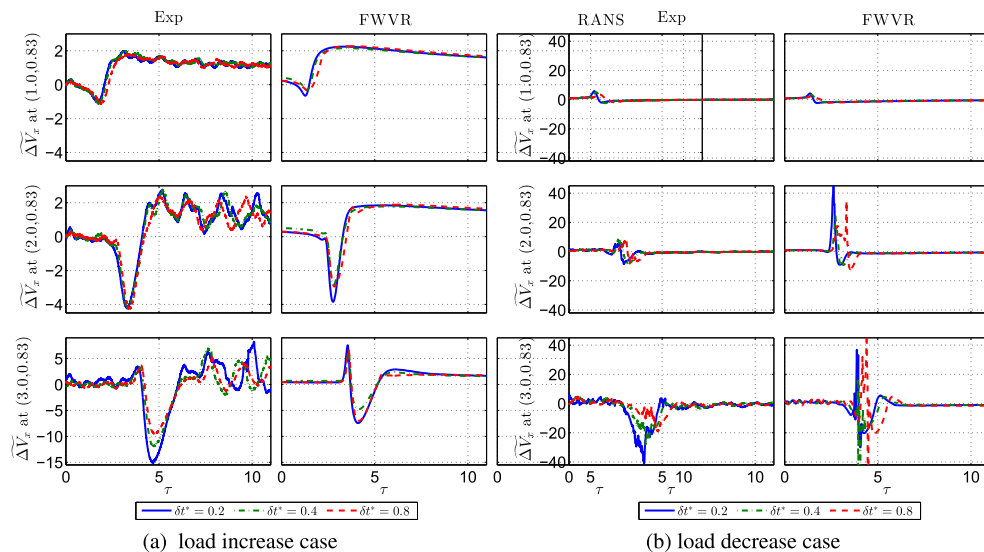

Fig. 13. Velocity at P4 ($z/D=1$, $y/D = 0.83$), P5 ($z/D=2$, $y/D = 0.83$), P6 ($z/D=3$, $y/D = 0.83$) from experiment and the FWVR model in load increase and decrease cases for $\delta t^* = 0.2$, 0.4, 0.8.

locations. This explains why the secondary unsteadiness at P4, P5 and P6 in the load decrease case is larger than that in the load increase case in Fig. 9. The reason is the same for that there is no or negligible peak in velocity at P1, P2 and P3 for load decrease case in Fig. 8(b).

The decomposed induced velocity at different locations shows that the secondary unsteadiness in velocity is determined by the effect of the passage of accumulated rolled-up vorticity and its relative distance to the observing locations during the process of convecting downstream. It presents as a velocity overshoot or undershoot or nothing under the combined effect. This verifies the hypothesis made in subsection 4.1.

4.3. The effect of reduced ramp time

This section compares the wake velocity profiles between the three unsteady load cases $\delta t^* = 0.2, 0.4, 0.8$.

Fig. 12 compares the velocity of the three reduced ramp time cases between the numerical and experimental results at P1, P2, P3 for load increase and decrease cases. In Fig. 12(a) and (b), it can be seen that the smaller the reduced ramp time, the larger the amplitude of velocity overshoot/undershoot, and the steeper slope of the transient velocity. For the experimental results, for all three cases, the difference is larger in the load decrease case than that in the load increase case. This may be caused by the stronger interaction of the rolled-up vorticity with the turbulence caused by the holes of the disc for the load increase case. In the load increase case, the vorticity moving inward results in higher turbulence in the inner wake.

Fig. 13 presents the velocity development at P4, P5 and P6 for load increase and decrease cases. The larger overshoot/undershoot and a steeper slope of velocity transient curve occurs for the smaller reduced ramp time case is also observed in the velocity profile for both the experimental and the numerical results.

Figs. 12 and 13 show that the numerical model can capture the overall trend of dynamic velocity profiles of the experiments for different reduced ramp time cases apart from some local amplitude difference. The main reasons causing the difference are the turbulence caused by the porous disc, effects of the hub, tower etc., which are not taken into account in the simulations. All these effects can affect the direct factor — the relative distances of rolled-up vorticity to the observed locations in the field during the process of convecting downstream, as discussed in subsection 4.2.

4.4. Decomposed velocity analysis of cases $\delta t^* = 0.2, 0.4, 0.8$

The difference in transient velocity for different reduced ramp time cases is discussed in subsection 4.3. The causes behind this difference are further explored by decomposing the velocity induced by different vortex elements from the FWVR model in this section.

Fig. 14 plots the decomposed induced velocity from the vortex shed after and before load change, the rolled-up vorticity and the total at P2 and P5, and the locations of the vortex rings at $\tau = 2.5$ after load increase for the three cases $\delta t^* = 0.2, 0.4, 0.8$.

It can be seen in Fig. 14(c) that the smaller the reduced ramp time, the larger extent of the rolling up process at the same time after the load change. In these load increase cases, the rolled-up

(a) Decomposed induced velocity at P2   (b) Decomposed induced velocity at P5

(c) Locations of vortex rings from the FWVR model for δt^*=0.2, 0.4, 0.8 at τ=2.5

Fig. 14. The velocity induced by the vorticity shed before and after load change, the rolled-up vorticity and the total at P2 ($z/D=2$, $y/D = 0.33$) and P5 ($z/D=2$, $y/D = 0.83$), and locations of the vortex rings of the FWVR model at $\tau = 2.5$ for load increase of cases $\delta t^* = 0.2, 0.4, 0.8$.

(a) Decomposed induced velocity at P2

(b) Decomposed induced velocity at P5

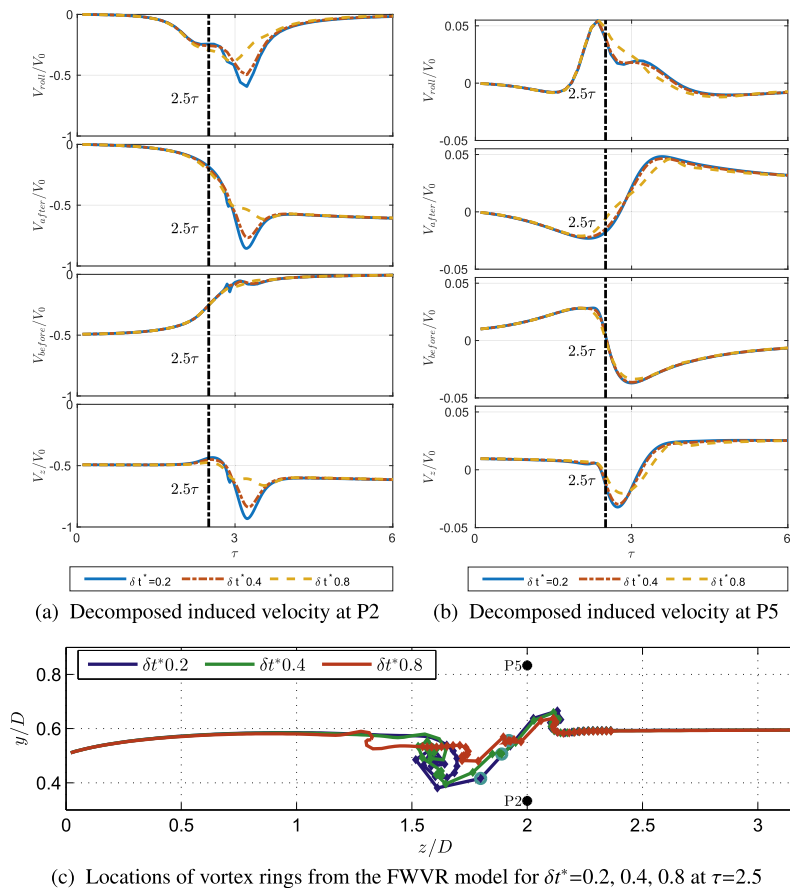(c) Locations of vortex rings from the FWVR model for δt^*=0.2, 0.4, 0.8 at τ=2.5
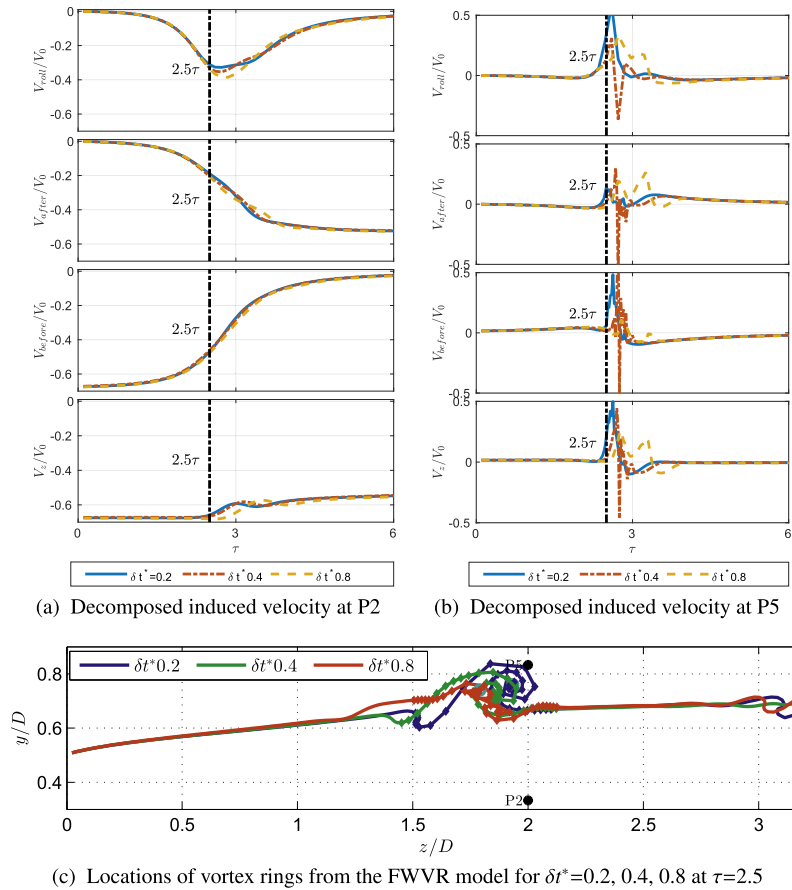
Fig. 15. The velocity induced by the vorticity shed before and after load change, the rolled-up vorticity and the total at P2 (z/D=2, y/D = 0.33) and P5 (z/D=2, y/D = 0.83), and locations of the vortex rings of the FWVR model at τ = 2.5 for load decrease of cases δt^* = 0.2, 0.4, 0.8.

vorticity moves inward. As a result, the vorticity moves towards to P2 but away from P5. Under the superposition effect of larger roll-up vorticity and smaller distance between the rolled-up vorticity to the observed locations, a smaller reduced ramp time leads to a larger peak of velocity at P2 induced by the rolled-up vorticity. Due to the counter effect of larger roll-up vorticity and larger distance between the rolled-up vorticity to the observed locations, there is no difference in the peak of velocity at P5 induced by the rolled-up vorticity between the three cases. In this load increase case, a slight difference of velocity induced by the vortex shed before load change at both locations because that few vortex elements shed before the load change are involved in the roll-up process. The smaller the reduced ramp time, the larger the amplitude of velocity at P2 and the steeper the slope of velocity at P5 induced by the vortex shed after load increase.

Fig. 15 presents the decomposed induced velocity from the vortex shed after and before load change, the rolled-up vorticity and the total at P2 and P5, and the locations of the vortex rings at τ = 2.5 after load decrease for the three cases δt^* = 0.2, 0.4, 0.8. Fig. 15(c) also shows a smaller reduced ramp time results in a larger extent of the rolling up process. The rolled-up vorticity moves towards to P5 but away from P2 due to the outward movement of the rolled-up vorticity in this load decrease case. By the superposition effect of larger roll-up vorticity and smaller distance between the rolled-up vorticity to the observed locations, a smaller reduced ramp time results in a larger peak of velocity at P5 induced by the rolled-up vorticity. Under the counter effect of larger roll-up vorticity and larger distance between the rolled-up vorticity to

the observed locations, a smaller reduced ramp time results in a smaller peak of velocity at P2 induced by the rolled-up vorticity.

5. Conclusions

The unsteady flow of an actuator disc during the transient load with different reduced ramp time has been investigated numerically with a free wake vortex ring model. A simple generic free wake vortex ring model is used to simulate the dynamic wake development. It is demonstrated that the vortex model is capable of capturing the dominant wake dynamics for steady and unsteady cases. For steady cases, the wake profiles between the numerical and experimental results are in good agreement, except for the wake boundary shear layer region. For unsteady cases, the secondary unsteadiness — overshoot/undershoot in velocity is observed in both the experiments and the numerical results. The discrepancy of velocity in the shear layer region between the numerical and experimental results suggests that the implementation of a viscous diffusion model can be a main improvement area.

It is found that the vortex sheet at the edge of the disc rolls up into a vortical ring structure gradually during the convecting downstream process after the disc load change. The vortex spirals inward in the load increase cases, spirals outward in the load decrease cases. It is further proved that the difference in wake velocity between the load increase and decrease cases is mainly caused by this different vorticity roll-up process.

This work also confirms that the extent of the rolling-up process and its relative distance to the observed points are the main reasons

causing the difference in velocity transient slope and difference in the amplitude of velocity peaks at the different observed locations, by utilizing decomposing velocity induced by different vortex elements.

The numerical model proves the effect of ramp time as observed in the experiments. A smaller reduced ramp time (a faster load change) leads to a steeper transient velocity change and in turn a larger amplitude of the velocity overshoot/undershoot. It is revealed that the different velocity profiles at the same location in the three reduced ramp time cases resulted from the different extent of the rolling up process, by decomposing the velocity induced by different vortex elements. A smaller reduced ramp time leads to a larger extent of the rolling up process.

Acknowledgments

References

[1] G. van Kuik, J. Sørensen, V. Okulov, Rotor theories by professor Joukowsky: momentum theories, Prog. Aero. Sci. 73 (2015) 1–18.
[2] R.E. Froude, On the part played in propulsion by differences of fluid pressure, Transact. Inst. Naval Arch. 30 (1889) 390–405.
[3] E. Callaghan, S. Maslen, The Magnetic Field of a Finite Solenoid, Tech. Rep, National Aeronautics and Space Admnistration, Lews Research Center, Ohio, 1960.
[4] I. Gibson, On the velocity induced by a semi-infinite vortex cylinder: with extension to the short solenoid, Aeronaut. J. 78 (762) (1974) 262–268.
[5] G. van Kuik, L. Lignarolo, Potential flow solutions for energy extracting actuator disc flows, Wind Energy 19 (2016) 1391–1406.
[6] E. Branlard, M. Gaunaa, Cylindrical vortex wake model: right cylinder, Wind Energy 18 (11) (2014) 1973–1987.
[7] J.T. Conway, Analytical solutions for the actuator disk with variable radial distribution of load, J. Fluid Mech. 297 (1995) 327–355.
[8] G. van Kuik, The edge singularity of an actuator disc with a constant normal load, in: 22nd AIAA/ASME Wind Energy Symposium, Reno, USA, 2003.
[9] S. Øye, A simple vortex model of a turbine rotor, in: Proceedings of the Third IEA Symposium on the Aerodynamics of Wind Turbines, Harwell, 1990, pp. 1–15.
[10] H. Madsen, A CFD analysis of the actuaotr disc flow compared with momentum theory results, in: 10th IEA Meeting on Aerodynamics, December, Edinburgh, 1996, pp. 109–124.
[11] R. Mikkelsen, Actuator Disc Methods Applied to Wind Turbines, Ph.D. thesis, Technical University of Denmark, 2003.
[12] L. Lignarolo, D. Mehta, R. Stevens, A. Yilmaz, G. van Kuik, S.J. Andersen, C. Meneveau, C. Ferreira, D. Ragni, J. Meyers, G. van Bussel, J. Holierhoek, Validation of four LES and a vortex model against stereo-PIV measurements in the near wake of an actuator disc and a wind turbine, Renew. Energy 94 (2016) 510–523.
[13] P. Koumoutsakos, D. Shiels, Simulations of the viscous flow normal to an impulsively started and uniformly accelerated flat plate, J. Fluid Mech. 328 (1996) 177–227.
[14] H. Higuchi, H. Balligand, Numerical and experimental investigations of the flow over a disk undergoing unsteady motion, J. Fluid Struct. 10 (1996) 705–719.
[15] W. Yu, V. W. Hong, C. Ferreira, G. van Kuik, Experimental analysis on the dynamic wake of an actuator disc undergoing transient loads, Exp. Fluid 58: 149.
[16] W. Yu, C. Ferreira, G. van Kuik, D. Baldacchino, Verifying the Blade Element Momentum Method in unsteady, radially varied,axisymmetric loading using a vortex ring model, Wind Energy 20 (2) (2016) 269–288.
[17] A. Pierides, A. Elzawawy, Y. Andreopoulos, Transient force generation during impulsive rotation of wall-mounted panels, J. Fluid Mech. 721 (2013) 403–437.
[18] A. Yang, L. Jia, X. Yin, Formation process of the vortex ring generated by an impulsively started circular disc, J. Fluid Mech. 713 (2012) 61–85.